Journal of Power Sources 198 (2012) 393–401

Contents lists available at SciVerse ScienceDirect

Journal of Power Sources

journal homepage: www.elsevier.com/locate/jpowsour

Nanotextured gold coatings on carbon nanofiber scaffolds as ultrahigh surface-area electrodes

Kevin M. Metz*, Paula E. Colavita[1], Kiu-Yuen Tse[2], Robert J. Hamers

Department of Chemistry, University of Wisconsin-Madison, 1101 University Ave., Madison, WI 53706, USA

ARTICLE INFO

Article history:
Received 3 August 2011
Received in revised form
28 September 2011
Accepted 28 September 2011
Available online 4 October 2011

Keywords:
Gold
Carbon
Electrodes
Nanoscale
Supercapacitor

ABSTRACT

High surface area metal electrodes are desirable for applications in energy storage and energy conversion. Here, the formation and electrochemical characterization of a hybrid material made by electroless deposition of gold onto a scaffolding of vertically aligned carbon nanofibers is described. Vertically aligned carbon nanofibers, ~80 nm in diameter, provided mechanical support and electrical contact to the highly textured nanoscale gold coatings. By chemically functionalizing the nanofiber surfaces and then using electroless deposition methods, a highly textured metal coating was formed. The electrochemical response of these "nano-on-nano" hybrid electrodes was characterized using electrochemical methods. The results show that using the metallic coatings can increase the electrochemically active surface area by up to a factor of 10 compared with the starting carbon nanofiber scaffolds. The electrochemical response of the electrodes was modulated by varying the deposition time of the gold.

1. Introduction

Recently high surface area materials, such as nano-composites, have received much attention as substrates for emerging energy storage and conversion technologies [1–3] associated with supercapacitors [4,5], next-generation batteries [6], fuel cells [7–9], and catalysis [10,11]. Nanoscale forms of carbon, including nanotubes and nanofibers, have been the focus of much research due to their excellent chemical stability and electrical conductivity [2,3]. Nanoscale forms of carbon can also be combined with polymers or metals to form nano-composites [3,7,9,12–16]. Such nano-composites are attractive because their properties can be altered, building from the excellent performance of the nanoscale carbon to create structures with tailored chemical or electrical properties [2,3]. However, fabrication of these composites can be hampered by the atomic perfection of nanoscale carbon, which can create non-reactive surfaces. For example, many types of nanoscale carbon need to be oxidized before metals can be deposited [13]. Often, the oxidation processes used are harsh and can damage, or destroy, much of the carbon. Additionally, accessibility of the full surface area can be difficult to achieve.

A gold–carbon nanocomposite based on vertically aligned carbon nanofibers (VACNFs) [17] has previously been reported on. The fabrication method takes advantage of the fact that nanofibers can be grown in a structure in which graphene sheets are nested inside one another in a stacked-cup arrangement. This structure exposes large amounts of edge-plane graphite along the sidewalls. Photochemical functionalization of the nanofibers with a molecular layer exposing carboxylic acid groups leads to extremely efficient nucleation of metals onto the nanofibers [17,18]. The use of photochemical functionalization has the advantage of being fully compatible with metal substrates and causing no damage to the physical properties of the nanofibers.

Previous studies also showed that metal deposition on top of the molecular monolayer modified VACNFS increased the active area of the electrode by a factor of 10 compared to the nanofiber template; creating an electrode with a 100 fold increase in electrochemically accessible surface area compared to a planar electrode [17]. Additionally, it was demonstrated that the effective capacitance of these highly textured electrodes scaled with the accessible surface area [17].

Here a more thorough characterization of Faradaic and non-Faradaic responses of these highly textured, nano-structured gold electrodes in order to understand the resulting interfacial electrical response. Data that helps elucidate the mechanism of the electroless plating on molecular monolayer-modified carbon surfaces is presented. Additionally, the electrical response of the electrodes

* Corresponding author. Present address: Department of Chemistry, Albion College, 611 E. Porter St., Albion, MI 49224, USA. Tel.: +1 517 629 0656; fax: +1 517 629 0264.
E-mail address: kmetz@albion.edu (K.M. Metz).
[1] Present address: School of Chemistry, Trinity College Dublin, College Green, Dublin 2, Ireland.
[2] Present address: 3M Company, Corporate Research Materials Laboratory, St. Paul, MN 55144-1000, USA.

0378-7753/$ – see front matter © 2011 Elsevier B.V. All rights reserved.
doi:10.1016/j.jpowsour.2011.09.098

at the interface of aqueous solution, both in the presence and absence of electron transfer reagents, is investigated. Finally, comparisons are made to other types of high surface area electrodes. The results demonstrate that metal-on-carbon hybrid nanostructures, which have a high surface capacitance and lower contact resistance, can provide very high surface area of electrochemically accessible, chemically stable materials that may be of potential utility in energy storage, e.g., as electrodes in electrochemical double layer capacitors [4].

2. Experimental

2.1. Growth of carbon nanofibers

Carbon nanofibers were grown in a custom built chamber using DC plasma enhanced chemical vapor deposition (DC-PECVD) [19–21]. Silicon substrates (with their native oxide) were coated with 50 nm of molybdenum, 20 nm of titanium, and 20 nm nickel as the top layer. Nanofibers were grown using acetylene and ammonia with flow rates of 30 standard cubic centimeters per minute (sccm) and 80 sccm, respectively, at a chamber pressure of 4 Torr and a DC power of 360 W. Growth times and conditions determine the physical properties of the nanofibers produced. Here, all fibers were grown for 15 min, which produces high densities of vertically aligned, cylindrical nanofibers with an average diameter of 80 nm and an average length of 2 μm.

2.2. Gold deposition on carbon nanofibers

To enhance nucleation of gold the nanofibers were functionalized with a molecular monolayer in order to produce a high density of carboxylic acid groups along the nanofiber sidewalls. This was achieved using a photochemical grafting procedure developed previously [22] in which organic molecules bearing a terminal alkene group (C=C) covalently grafts to the graphitic edge-planes of VACNFs when illuminated with ultraviolet light at 254 nm [23]. This method has been shown to form molecular layers that allow facile electron transport [24]. Here, this work is extended to metallic layers on carbon nanofibers. Freshly grown VACNFs were reacted with undecylenic acid methyl ester by dripping a thin film of the pure liquid reagent onto the VACNF samples, and illuminating with 254 nm light ($\sim$1 mW cm^{-2}) for 16–18 h in a nitrogen-purged reaction chamber. The surface-linked ester was then converted to carboxylic acid using a slurry of potassium tert-butoxide in dimethyl sulfoxide [24], producing carbon nanofibers functionalized with carboxylic acid moieties. The fibers were then cleaned in 0.1 M HCl and washed in a 50:50 solution of distilled water and methanol.

Deposition of gold onto the COOH-terminated nanofibers [17] was achieved by sensitizing the carboxylic acid-modified fibers in a bath containing 0.026 M $SnCl_2$ and 0.07 M trifluoroacetic acid in a 50:50 methanol: deionized water solution; this step binds tin ions to the carboxylic acid moieties on the surface [25]. The tin sensitized fibers were then activated with silver by immersion in a silver bath consisting of 0.03 M ammoniacal silver nitrate. This leaves atomic silver bound to the surface, via a redox reaction with the tin ions. Finally the VACNF samples were placed in individual gold baths, containing 0.127 M Na_2SO_3, 0.025 M $NaHCO_3$, 0.625 M formaldehyde and 8 mM $Na_3Au(SO_3)_2$ (Technic Oromerse Part B gold solution), at pH 10, and 6 °C for durations of 1–22 h. The time in the gold bath controlled the amount of gold on the fibers [17].

2.3. Electrical characterization

Electrical characterization was carried out using electrochemical impedance spectroscopy (EIS) and cyclic voltammetry (CV) using a three-electrode geometry. Measurements were made in aqueous solutions of KCl, $KClO_4$, and $Ru(NH_3)_6^{+2/+3}$, of various concentrations. All measurements used the gold-coated carbon nanofiber sample as the working electrode. For comparison, capacitance measurements were made in aqueous solutions of KCl over planar gold and glassy carbon electrodes. The data were collected using a single junction Ag/AgCl (3 M KCl) reference electrode. In all measurements ohmic contact was made to the top side of the gold-coated carbon nanofiber samples outside of the fluid compartment of the cell. Impedance measurements were made at the open circuit potential in room temperature. Aqueous solutions were purged

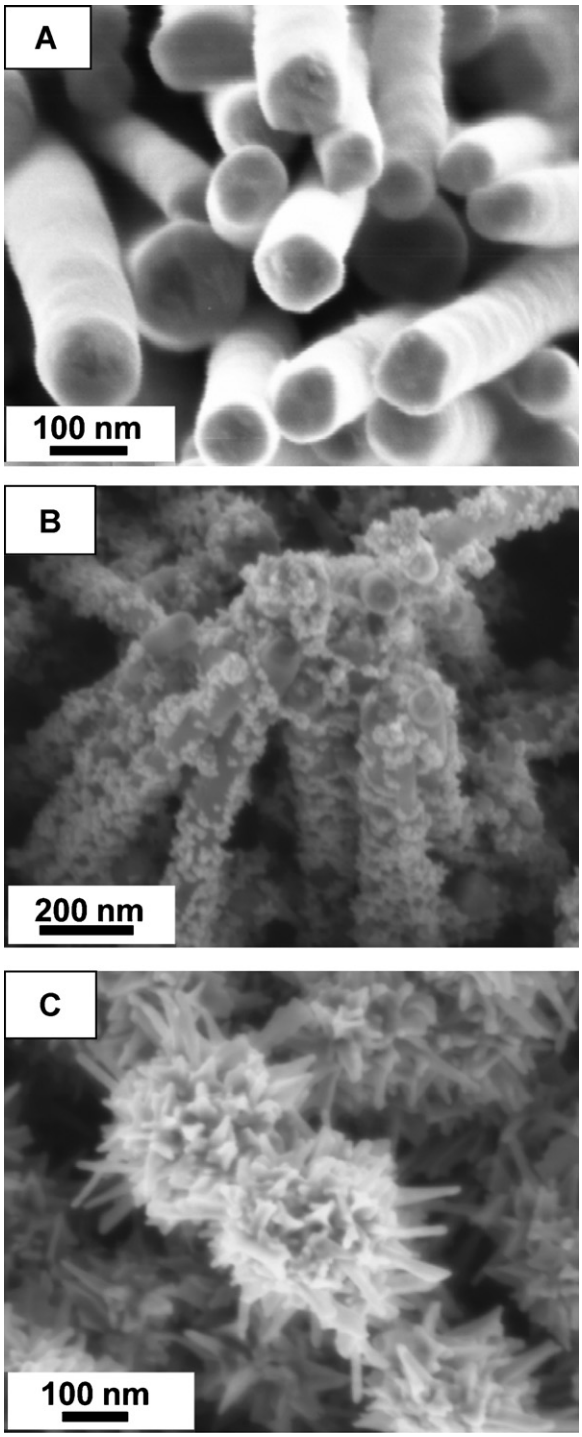

Fig. 1. Scanning electron microscopy images of carbon nanofibers (A) before gold bath, (B) after 3 h in a gold bath and (C) after 7 h in a gold bath.

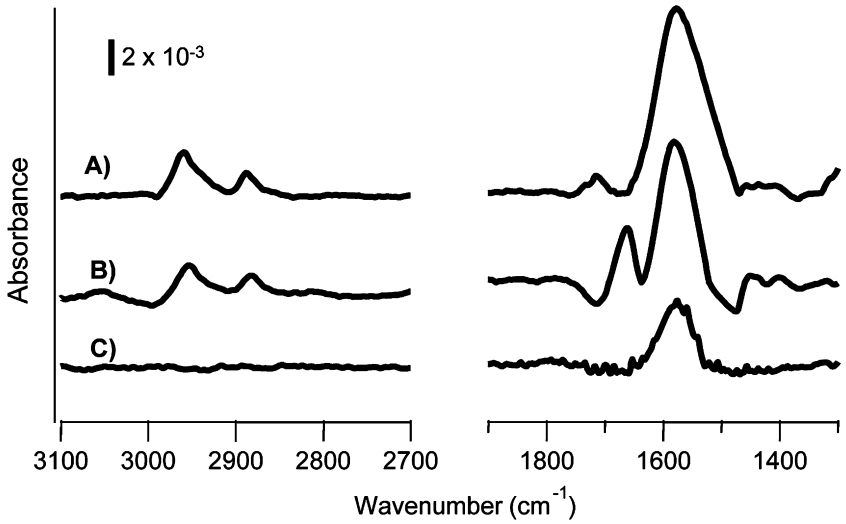

Fig. 2. Fourier transform infrared (FTIR) spectra of carbon nanofibers: (A) functionalized with carboxylic acids, (B) functionalized with carboxylic acids and exposed to tin and (C) control sample without functionalization but exposed to tin.

with argon prior to use. All data shown here have been normalized to the geometric area of the cells used. All measurements were performed using a 3-electrode potentiostat and impedance analyzer (Solartron 1260/1287) using Zplot or Corrware software (Scribner Associates, Inc.).

2.4. Fourier transform infrared (FTIR) measurements

The chemical functionalization and tin sensitization of the carbon nanofibers were verified using infrared spectroscopy. Spectra were collected using infrared reflection absorption spectroscopy (IRRAS) in a Bruker Vertex 70 FTIR spectrometer with a variable angle reflection accessory (VeeMaxII, Pike). Spectra shown here were collected with s-polarized light at an incidence angle of 60° from the surface normal. The background and sample spectra each consisted of 500 scans at 4 cm^{-1} resolution. Spectra were baseline-corrected using commercial software (Grams, Thermo Galactic).

3. Results

3.1. Nanoscale morphology

Fig. 1 shows scanning electron microscope (SEM) images of as-grown VACNFs before any modification (Fig. 1A) and functionalized nanofibers after immersion in the gold deposition bath for different lengths of time. It is clear from Fig. 1A that the fibers are cylindrical, vertically aligned and packed in a high density arrangement. Once functionalized and placed in a gold bath, nanoparticles of gold nucleate grow on the carbon nanofibers. Fig. 1B shows VACNFs after 3 h in a gold bath. At this point the nanoparticles are clearly visible and in some cases have started to coalesce. After 5 h in the gold bath the gold nanoparticles have fully coalesced, forming a textured gold sheath that completely encapsulates the carbon nanofibers. With continued time in the gold bath, the gold sheath forms a more complex texture, with spike-like features frequently extending more than 100 nm long. Fig. 1C shows a gold–carbon composite after 7 h in a gold bath, which displays this complex, highly textured gold coating. The interactions of the spike-like projections on neighboring fibers form a very complex, essentially random network in the interstitials between the fibers.

Control experiments were performed on planar carbon surfaces that were functionalized with an identical monolayer. The functionalized planar surfaces showed a high density of nanocrystalline gold particles and some regions of spongy masses of gold, but did not show the complex morphology observed on the functionalized VACNFs.

3.2. Characterization of functionalization chemistry and impact on electroless deposition on VACNF electrodes

An important aspect of the fabrication method is the use of a molecular layer to provide carboxylic acid sites for metal binding. Infrared spectroscopy was used to characterize the chemical changes associated with the functionalization and their influence on the final structures shown in Fig. 1. Fig. 2 shows infrared absorption spectra of carbon nanofibers that were photochemically functionalized and de-protected to expose carboxylic acid groups before (Fig. 2A) and after (Fig. 2B) exposure to tin. Fig. 2C shows a control spectrum for a carbon nanofiber sample that was not functionalized, but was exposed to the tin sensitization bath. The absorption band of atmospheric carbon dioxide near 2360 cm^{-1} has been omitted for clarity. All spectra were collected and referenced to a background spectrum collected from a freshly grown, bare carbon nanofiber sample using a 60° incidence angle and s-polarized light.

All three spectra are dominated by a large peak near 1587 cm^{-1}; this peak appears to originate in C=C binding vibrations of the bulk nanofibers and thus is related to the nanofiber structure. Therefore examination of changes in the weaker features in the spectra is needed to monitor changes in the surface chemistry. The FTIR spectrum shown in trace (A) of Fig. 2 shows methylene (CH_2) peaks at 2927 and 2856 cm^{-1} and a sharp peak in the C=O regions at 1715 cm^{-1} [26].

The importance of surface chemical termination is revealed more clearly after the next step of functionalization, which involves binding of tin as a sensitizer to the nanofibers. Tin exposure was carried out by wetting the fibers with methanol and then soaking them in the tin sensitizing bath for 30 min. The spectrum of the "bare" nanofibers that was exposed to tin shows no significant features other than the peak near 1587 cm^{-1}, which corresponds to the bulk nanofibers. For the COOH-modified samples (Fig. 2b), exposure to tin leads to no significant change in the C–H region, but the peak at 1715 cm^{-1} (2A) disappears and is replaced with a new peak at 1658 cm^{-1} (2B). This is very close to the value of 1655 cm^{-1} previously reported for the C=O antisymmetric stretching of tin carboxylate [27].

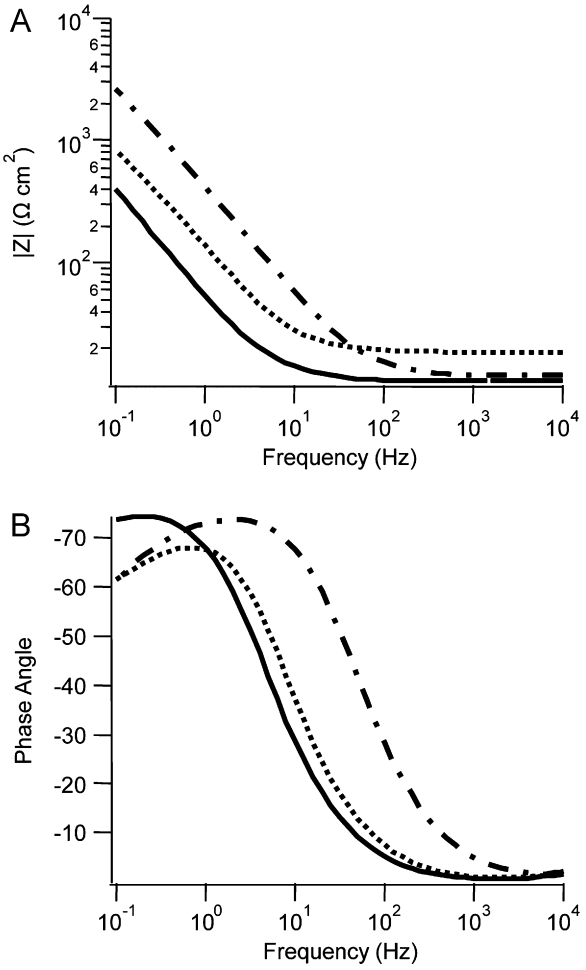

Fig. 3. (A) Absolute impedance and (B) phase angle as a function of frequency, measured at the open circuit potential in 0.1 M KCl for bare carbon nanofiber (dash-dotted line), carbon nanofibers after 3 h gold deposition (dotted line) and carbon nanofibers after 7 h gold deposition (solid line).

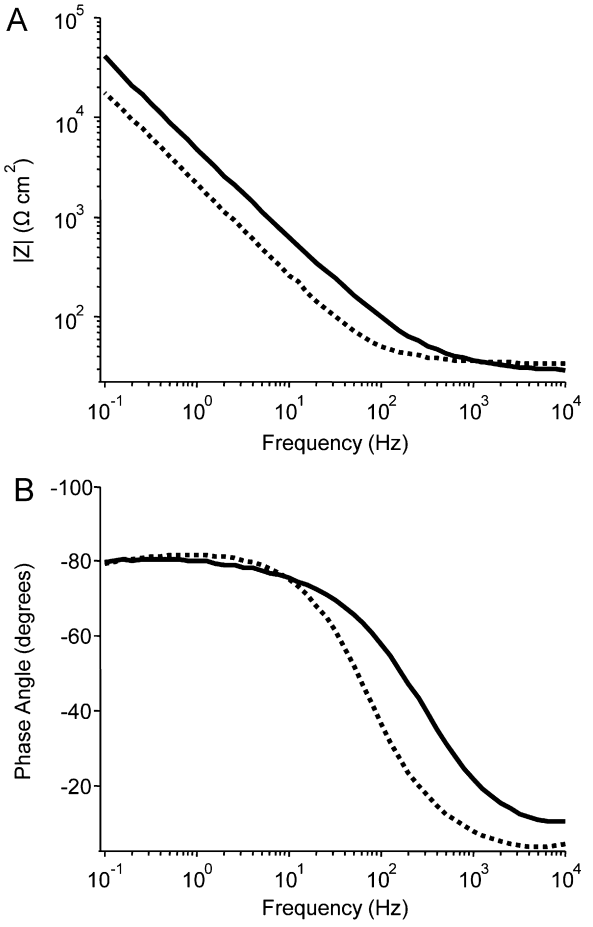

Fig. 4. (A) Absolute impedance and (B) phase angle as a function of frequency, measured at the open circuit potential in 0.1 M KCl for glassy carbon (solid) and gold (dotted) planar electrode.

The FTIR data show that (1) photochemical functionalization leads to formation of stable monolayers and (2) that immersion into the tin bath leads to clear, well-defined changes in the spectra corresponding with the transition from –COOH termination to $-(COO^-)_2Sn^{2+}$. Finally, the fact that no significant CO features are observed on the "bare" nanofibers either before (data not shown) or after tin treatment demonstrates that the bare nanofibers have only small numbers of carboxylic acid groups, below the detection limit of FTIR. The fact that there is no corresponding peak in the bare nanofibers spectrum provides direct evidence that the molecular layer is needed to create oxidized carbon sites for metal binding (*vide infra*).

3.3. Electrochemical impedance measurements

Electrochemical impedance spectroscopy (EIS) was used to examine how the evolution in morphology from the simple cylinders to the more complex geometry visible in Fig. 1 alters the electrical properties of the interface. In EIS, a small modulation with a root-mean-square (RMS) amplitude of ~10 mV is applied to the sample. The in-phase and out-of-phase components of the current are measured, and the impedance is described by the complex quantity

$$Z = Z' + iZ'' \quad (1)$$

Impedance data are usually presented as plots of the magnitude ($|Z|$) and phase angle (θ) of the impedance as a function of frequency. Fig. 3 shows EIS on bare carbon nanofibers and on carboxylic acid-modified nanofibers that were exposed to the gold electroless deposition bath for 3 h and 7 h. These measurements were made in 0.1 M KCl solution at the open circuit potential (0.086 V, 0.023 V, and 0.044 V vs. Ag/AgCl for the bare, 3 h and 7 h samples respectively). At low frequencies, all three samples show nearly linear decreases in impedance, dropping over the range from 0.1 Hz to 10 Hz. Fig. 3A shows that increased time in the gold bath results in a lower impedance at low frequency. At 0.1 Hz, the lowest frequency measured here, the absolute impedance drops from ~2600 Ω cm^2 for bare nanofibers, through ~820 Ω cm^2 for nanofibers with gold deposited 3 h to a minimum of ~400 Ω cm^2 for nanofibers with 7 h of gold deposition, representing a ratio of impedances of ~1.0: 0.31: 0.15. This ratio of impedances is over the frequency range from 0.1 Hz to 10–100 Hz. At high frequency, greater than 1 kHz, the area-normalized impedance of all three samples drops to a few Ω cm^2. This impedance corresponds to the uncompensated resistance of the solution. While this uncompensated resistance should be the same for all samples, some variations arise due to slight irreproducibility in the position of the reference electrode, as verified by independent control experiments.

Fig. 3B shows that increased time in the gold bath also results in a larger phase angle. A phase angle of −90° corresponds to ideal capacitance, whereas a phase angle of 0° corresponds to pure resistance. All three samples show roughly sigmoidal shaped curves as a function of frequency. Bare nanofibers and 3 h gold-coated

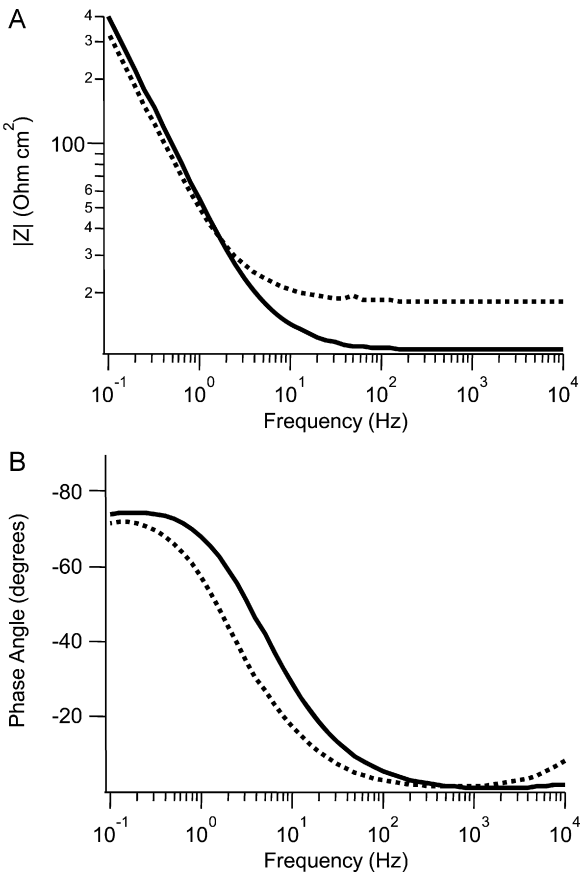

Fig. 5. (A) Absolute impedance and (B) phase angle as a function of frequency, measured at the open circuit potential in 0.1 M KCl (solid), 0.1 M $KClO_4$ (dotted) on a 7 h gold-coated carbon nanofiber electrode.

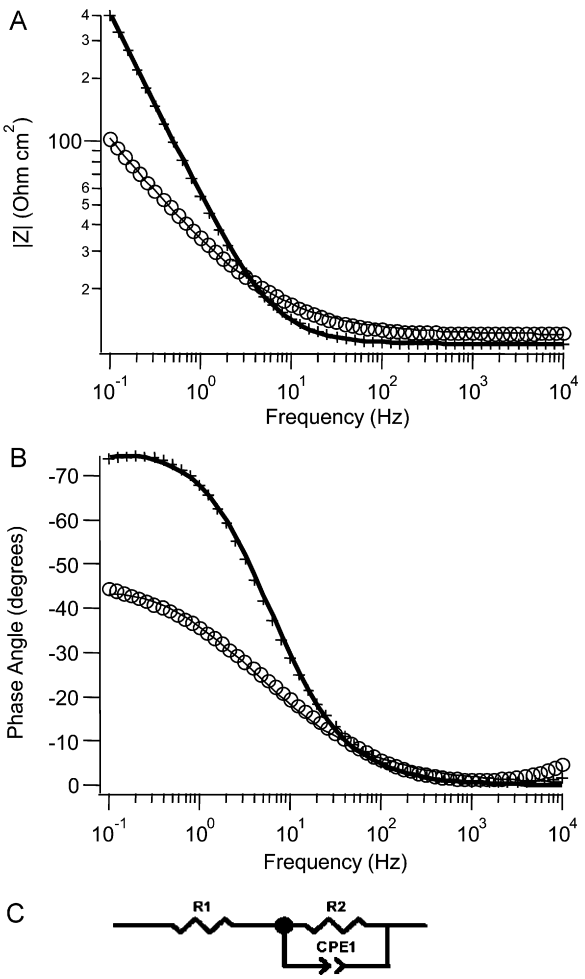

Fig. 6. (A) Absolute impedance and (B) phase angles response as a function of frequency for a 7 h gold-coated carbon nanofiber electrode in 100 mM KCl (crosses) and in 4 mM $Ru(NH_3)_6$ in 100 mM KCl (circles). The lines represent fits calculated using the (C) equivalent circuit model.

nanofibers show a phase angle of approximately −60° at 0.1 Hz while nanofibers with 7 h of gold deposited on them show a phase angle of −74°. All three curves shift upwards, toward −90°, before falling to near 0° at frequencies around 1 kHz. This higher phase angle observed at low frequency implies that with the addition of more gold, the fibers become slightly more ideally capacitive.

The formation of the highly textured gold surfaces is accompanied by a change in the electrode material (carbon to gold) and in the effective area in contact with the electrolyte solution. In the case of carbon based electrodes, the capacitance further depends on the ratio of basal-plane to edge-plane graphite present [28,29]. To help determine how each of these factors contributes to the changes in impedance, EIS measurements were made on planar glassy carbon and planar gold electrodes in 0.1 M KCl solutions. Glassy carbon was selected as planar comparison because it contains a large amount of edge-plane graphite [30], much akin to the carbon nanofibers.

Fig. 4 shows the impedance and phase angle vs. frequency for these samples. At the lowest frequencies (0.1 Hz) the impedances for gold and glassy carbon samples are both substantially larger than those observed with nanofiber samples. In both cases, the total impedance drops nearly linearly from 0.1 Hz to ~10^2–10^3 Hz, and at higher frequencies plateaus at a constant value corresponding to the uncompensated solution resistance. The phase angle data, Fig. 4B, again exhibit roughly sigmoidal shapes, reaching phase angles of −80° at the lowest frequency, increasing very slightly toward 90°, and then at a frequency of 10^2–10^3 Hz dropping toward zero. Fig. 4A shows that the glassy carbon electrodes display approximately twice the impedance of the gold sample. This difference likely arises from a combination of factors including an increased density of states and higher roughness for the gold sample and indicates that the much more pronounced difference observed in comparing bare VANCFs with gold-covered VACNFs is primarily geometric in origin, but may have some contribution from the difference in materials

Another possible contributor to the absolute impedance observed with the addition of gold to carbon nanofibers is the high specific adsorption of chloride ions to gold [31]. To help separate the effects of surface area and specific adsorption, experiments were performed changing the composition and concentration of the electrolyte concentration. Since potassium perchlorate ($KClO_4$) does not exhibit strong adsorption to gold [32], data in chloride- and perchlorate-containing solutions can be used to assess whether there is strong specific adsorption to the gold surfaces. Fig. 5 shows absolute impedance and phase angle data for gold coated carbon nanofibers in 0.1 M KCl and 0.1 M $KClO_4$ measured at the open circuit potential. The spectra in Fig. 5 are not significantly different from one another; this demonstrates that the impedance behavior of the Au-coated fibers is not dominated by anion adsorption effects.

3.4. Charge transfer at electrodes

To determine how the nanotextured gold coating impacts the electron-transfer properties of the sample, Faradaic processes at the surfaces using the redox couple $Ru(NH_3)_6^{2+/3+}$ were examined. Previous studies have shown that $Ru(NH_3)_6^{2+/3+}$ is an outer-sphere

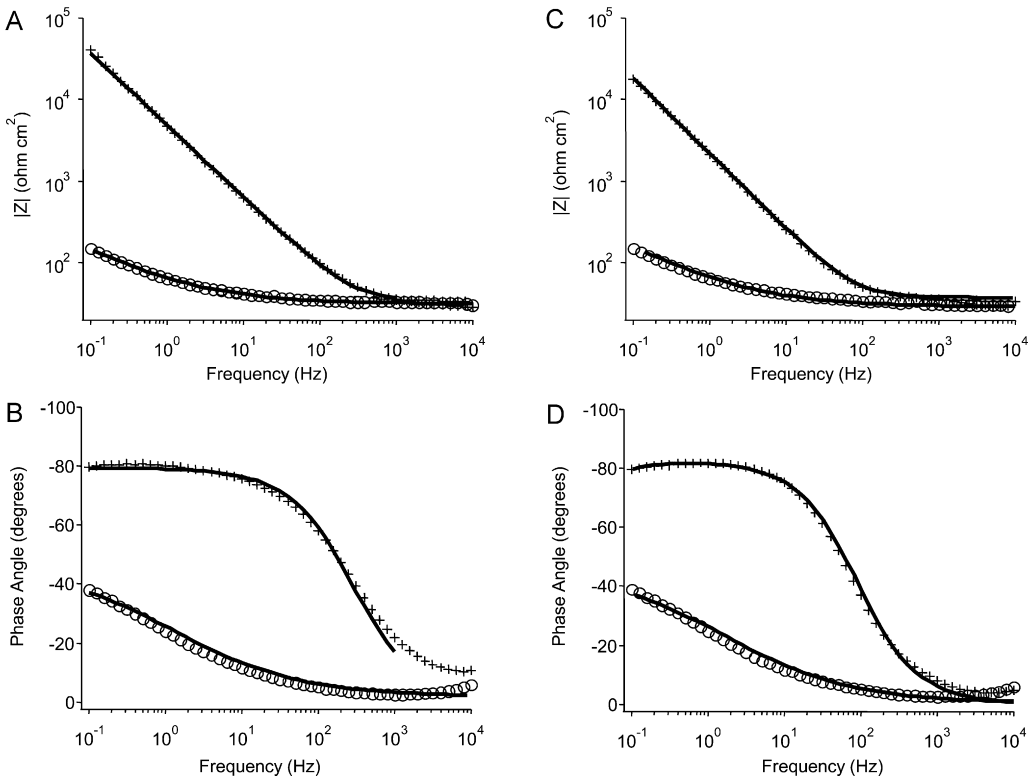

Fig. 7. Absolute impedance and phase angle as a function of frequency, in 0.1 M KCl (crosses), and 5 mM $Ru(NH_3)_6^{2+/3+}$ in 0.1 M KCl (circles) on glassy carbon (A and B) and gold (C and D) planar electrodes. Line represent fits to the data calculated using the equivalent circuit model in Fig. 6C.

system involving electron transfer that is sensitive primarily to the density of states of the electrode, and relatively insensitive to surface chemical composition [33]. Fig. 6 shows the magnitude and phase of the impedance measured on an electrode with gold deposited on it for 7 h in 0.1 M KCl, and in a solution of 0.1 M KCl with 5 mM each of $Ru(NH_3)_6^{2+}$ and $Ru(NH_3)_6^{3+}$, collected at the open circuit potential. A fit to an equivalent circuit model, is also shown. The equivalent circuit used to construct this fit is shown in Fig. 6C, and consists of a resistor, modeling the solution resistance, in series with the parallel combination of a CPE and a resistor, which model the capacitance and charge transfer at the interface. The parameters used in the modeling are presented in Table 1.

Fig. 6A shows that above ~100 Hz, the presence of the redox agent has no significant change on the electrical response. At lower frequencies, however, the magnitude of the impedance is reduced. For example at 0.1 Hz the absolute impedance decreases from ~400 to ~100 Ω cm^2. The phase angle response (Fig. 6B) takes on a new shape in the presence of the redox couple, changing from the roughly sigmoidal shape observed in 0.1 M KCl to a more linear response at low frequency, falling from about −45° at 0.1 Hz to roughly 0° at 100 Hz. This is consistent with the fact that the impedance at these frequencies is limited by the uncompensated solution resistance, which is mostly unchanged by the addition of a low concentration of redox couple to the 0.1 M KCl solution.

As a point of reference, Fig. 7 shows impedance and phase angle data for planar glassy carbon and gold electrodes in 0.1 M KCl and in 0.1 M KCl containing 5 mM each of $Ru(NH_3)_6^{2+}$ and $Ru(NH_3)_6^{3+}$, measured at the OCP. Fig. 7 shows that, much akin to the behavior of the gold-modified carbon nanofibers, the addition of a redox couple significantly lowers the absolute impedance and phase angle of the planar electrodes at low frequency. However, the effect is much more dramatic with the planar samples. For example, at 0.1 Hz the hexaammineruthenium complex causes the impedance of the glassy carbon electrode to decrease from ~173 kΩ cm^2 to ~150 Ω cm^2 and the impedance of the gold electrode to drop from ~18 kΩ cm^2 to ~150 Ω cm^2.

One of the most significant results from these studies is that while for planar electrodes the redox agent reduces the impedance by a factor of more than 100, on gold-coated nanofibers the reduction is much smaller. This implies that the high surface area of the nanofibers is not the limiting factor in the Faradaic processes.

To explore the kinetics under quasi-steady state conditions, Fig. 8 shows cyclic voltammograms of gold coated carbon nanofibers (Fig. 8A) and a planar gold electrode (Fig. 8B) in a solution of 5 mM each of $Ru(NH_3)_6^{2+/3+}$ with 0.1 M KCl, at a scan rate of 25 mVs^{-1}. The shapes of the curves are different near the most positive and most negative potentials. This shape difference arises from the capacitance charging of the surface during the measurement.

Table 1
Equivalent circuit model (Fig. 7C) parameters for a 7 h gold-coated carbon nanofiber electrode, a planar gold electrode and a planar glassy carbon electrode in 0.1 M KCl and 5 mM $Ru(NH_3)_6^{2+/3+}$ in 0.1 M KCl.

Model component	Gold-CNF		Gold foil		Glassy carbon	
	KCl	$Ru^{2+/3+}$	KCl	$Ru^{2+/3+}$	KCl	$Ru^{2+/3+}$
R_s (Ohm)	11	12	35	32	34	33
R_{ct} (Ohm)	6.9×10^3	8.1×10^2	3.5×10^6	1.6×10^{11}	3.3×10^{13}	1.1×10^{11}
CPE T	0.0038	0.0129	8.7×10^{-5}	0.01	4.1×10^{-5}	0.01
CPE φ	0.88	0.59	0.92	0.50	0.88	0.50

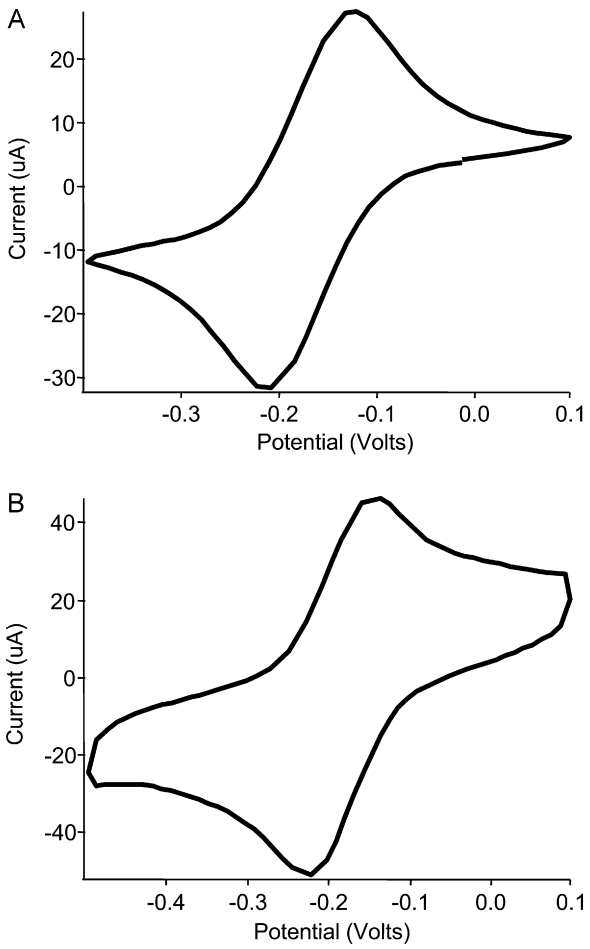

Fig. 8. Cyclic voltammograms collected in 5 mM $Ru(NH_3)_6^{2+/3+}$ in 0.1 M KCl at 25 mV s^{-1} over (A) a planar gold electrode and (B) a 7 h gold-coated carbon nanofiber electrode.

Fig. 8B also shows a peak current nearly twice as large as Fig. 8A, however calculating the area from the peak current, after removing the capacitive current contribution, results in the geometric area of the cell used here. This indicates that the gold coated nanofibers are in a planar diffusion regime. Diffusion effects may also be responsible for the increased peak separation. It is reasonable that diffusion effects seem to dominate given the very complex, nearly random networks that exist between the individual fibers.

4. Discussion

4.1. Materials requirements for metal–nanofiber composites

Recent studies have emphasized that high surface area, well-defined porosity and high crystallinity are indispensable requirements for materials in many energy storage and conversion applications [9]. For metals, high crystallinity implies good conductivity, and the high surface area with well-defined porosity implies a highly accessible surface area.

Previous studies on high surface area porous carbon have shown that the very small pores, which lead to high surface area, are not always accessible and can have difficulty supporting well defined electrical double layers [5]. Carbon nanotubes and nanofibers have emerged as novel high surface-area materials of intense interest. However, one problem with small-diameter (e.g., single-walled) carbon nanotubes is that their atomic structure is based upon wrapping of graphene sheets in such a manner that they expose almost entirely basal-plane graphite along their sidewalls.

In contrast, nanofibers grown by the methods used here expose large amounts of edge-plane graphite. In nanocarbons, such as single walled nanotubes and nanofibers, the activity is often increased by harsh oxidation procedures such as boiling in hot nitric acid, which creates defects and partially oxidizes the materials [13].

Another approach to increasing the surface area is to use nanostructures as a template for other materials, such as metals. This is particularly attractive for applications such as electrocatalysis, where the high surface area and tunable chemical reactivity of the metals can both be used. However, the results demonstrate that even noble metals such as gold can provide significant increases in the accessible surface area that could be used to practical advantage. VACNFs have been shown to increase the surface area of an electrode by at least 7 times [34]. This results from the well defined cylindrical geometry that VACNFs assume. Each fiber in a VACNF electrode also has the added benefit of an individual contact to the underlying electrode as a result of the growth mechanism. Thus VACNFs by themselves meet the requirements for materials applications in energy storage and conversion, making them an ideal choice for modifications.

4.2. Surface modification

One key issue in forming metal nanocomposites on carbon surfaces is the adhesion of the metals to the carbon surface. This is typically enhanced by oxidation of the surface using strong oxidizing acids, such as HNO_3. While this procedure can be effective, especially for bulk high surface-area carbons, it also has a few drawbacks. First, wet-chemical oxidation leads to a broad distribution of different types of oxidized carbon, only some of which are effective at binding to metals. This can be problematic for nanostructured carbon materials. Secondly, the harsh oxidizers are difficult to integrate with many metals commonly used as electrode materials. In contrast, the FTIR data show that the molecular functionalization with only carboxylic acid moieties was achieved on the surface under extremely gentle conditions, using 254 nm light to trigger the reaction.

One issue of initial concern was whether the molecules would act as insulators, adding a series resistance to the nanofiber–metal interface. However, the results suggest that any such resistances are negligible. These results are also consistent with previous results [34–36] using several different molecules, in each case showing that although the molecular densities are relatively high, the layers are sufficiently porous that good electrical contact is still made between the nanofiber and the metal electrode. Thus, the molecular monolayer can be used to enhance metal adhesion to the nanofibers without adversely affecting the electrical properties.

4.3. Surface texture

While the use of molecular monolayers provides a high density of chelating sites for metal deposition, the electroless deposition process results in a surprisingly corrugated surface texture. Electroless metal deposition generally results in smooth films [37]. Textured structures similar to those reported here have been reported previously from electrochemical deposition onto highly oriented pyrolitic graphite (HOPG) [38–40], with dendritic gold nanoparticles nucleating at step edges of the HOPG. Steps on HOPG reveal atomic structures essentially identical to those of the edge planes exposed every ~2–3 nm along the VACNFs.

In these previous studies, the highly textured geometry has been attributed to anisotropic diffusion of gold on different crystal planes, which can depend strongly on the types of ions in solution. Similar spike-like coatings, or dendritic coatings, can be formed by

electroless deposition, but usually only under fast deposition conditions. That is, conditions of high pH, elevated temperatures, or large metal concentrations [41–43]. Under these conditions the deposition reactions are fast and diffusion limited aggregation generally dominates the growth, resulting in a more fractal looking structure [42,43].

The method reported here is not operating under these conditions. Similar electroless gold deposition protocols used on porous polymer surfaces [25,44,45], as well as planar polymer and glass surfaces [46] have not reported any spike-like textures with their deposits. Additionally, control experiments performed in on planar glassy carbon, using identical procedures as described above, did not result in any highly textured deposits. While the formation of this highly textured coating remains not fully understood, it appears that the highly textured coating leads to many of the observed electrochemical properties of the electrodes.

4.4. Electrochemical behavior of the textured surface

Understanding the electrochemical behavior of gold surface is essential to understanding and predicting the response of the electrodes. Electrodes of this nature generally are either treated as rough electrodes and described by distributed elements such as a constant phase element (CPE) [47], or they are treated as porous electrodes and described with a transmission line model (TLM) [48], in which the impedance of a pore is defined in terms of an infinitely long transmission line defined by the solution resistivity and the impedance of the wall–electrolyte interface [48–50]. The distinction as to which of these two models is most appropriate is based on the depth of the pores relative to an effective penetration depth that describes how far an AC electric field penetrates into the pores [48–50]. The depth of the "pores" is ~2 μm. In this size range, the TLM model collapses to a rough electrode model [49] and a simple distributed element, such as a constant-phase element, is a better choice than the TLM for modeling the electrical properties of the system [47].

The CPE is defined via the impedance relationship $Z_{cpe} = 1/T(i\omega)^{\varphi}$, where T and ϕ are parameters. A perfect capacitor has $T = C$ and $\phi = 1$; deviations from these values can reflect a variety of non-ideal properties including microscopic roughness, electrical inhomogeneties at the interface, or diffusion limits to the electrode [47,51,52]. An electrode that shows deviations based solely on diffusion limited effects has an exponent equal to 0.5 [52]; exponents between 0.5 and 1 are often attributed to roughness effects [47,51]. It is likely that the complex shape of the electrodes leads to a combination of these effects.

Table 1 summarizes the parameters determined by fitting the data with an equivalent circuit consisting of a resistor in series with the parallel combination of a CPE and a resistor. It is clear from Table 1 that the samples show a significant deviation from ideal capacitance ($\phi = 1$). If the electrodes were behaving as true porous systems with diffusion occurring primarily between fibers down the length of the pore, one would expect an exponent value of 0.5 [52]. Diffusion occurring between a rough surface and the solution should result in an exponent between 0.5 and 1 [47,51]. Thus, the exponent of 0.88 obtained for the gold-coated nanofiber electrodes in 0.1 M KCl implies that the microscopic surface roughness associated with the network of gold influences the response of the electrodes, rather than diffusion between individual fibers in this system. Table 1 also shows that when the electrolyte concentration is kept constant but a redox agent is added, the charge-transfer resistance drops significantly, and the exponent value changes from 0.88 to 0.59. This change in the exponential value suggests a transition from complex behavior to more diffusion limited behavior in the presence of a redox agent, given that exponential values of 0.5, generally indicate diffusion limited behavior.

Calculations of active surface area based on the measurements in the presence of a redox couple show an area equivalent to the projected area of the electrode, rather than the extended area of the length of the fibers enhanced by the microtextured gold coating. This supports the hypothesis that diffusion occurs primarily between the nanofibers and the solution, and this limits the performance of the electrode in the presence of a redox couple. It should also be pointed out that the deviation from ideal capacitive behavior observed for gold coated carbon fibers is not significantly different from the deviation observed for bare carbon nanofibers with no gold coating, in KCl solutions [53]. The similarity in exponents between "bare" and gold-coated nanofibers implies that the deviation from "ideal" behavior is associated primarily with the nanofibers and not with the smaller-scale structure of the gold. This implies that the active surface area can be increased, without significantly altering the frequency response of the electrode, by the addition of gold in the absence of charge transfer.

The very high surface area provided by gold coating leads to interesting properties that could potentially be useful for applications such as energy storage in electrochemical double-layer capacitors [1]. Assuming a series RC model, the effective capacitance of the system can be extracted from the impedance using

$$C = \frac{-1}{2\pi f Z \sin\ \theta} \tag{2}$$

The high surface area obtained after 7 h of gold deposition, leads to an effective capacitance of 3.25 mF cm^{-2} [17]. This is a substantial increase compared to the average effective capacitance of 290 mF cm^{-2} for bare nanofibers in the same solution [17]. The value of 3.25 mF cm^{-2} is comparable to that obtained from rough porous gold electrode produced by leaching out a component from a gold alloy [54]. The short nanofibers investigated here yield capacitance values that are slightly smaller than the values of ~0.5–50 mF cm^{-2} obtained from high surface-area activated carbon electrodes in aqueous solution of KOH [5,55]. Nonetheless, the combination of highly textured gold on top of carbon nanofiber scaffolding presents a unique material that can be customized for different applications.

5. Conclusions

A new fabrication method for producing tunable nanoscale gold–carbon composite electrodes has been demonstrated. The method utilizes molecular functionalization, developed for planar carbon materials, to provide a high density of carboxylic acid binding sites uniformly distributed along the length of the carbon nanofiber starting materials. This approach avoids strong oxidants, making this method fully compatible with metal substrates. The deposition process allows for control over the amount of gold added to the surface. The resulting electrodes show high accessibility in aqueous solutions. This method should be extendible to different metals, allowing for the creation of electrodes for use in a variety of applications including energy conversion and electrocatalysis.

The tunable nature of the metal deposition process can lead to useful substrate materials ranging from highly disperse particles of metal [18], useful in applications such as fuel cells and catalysis, to the full, highly textured coatings studied here. Gold has been shown to be catalytically active when present in the nanoscale [11,56,57]. Nanoscale gold has also attracted attention recently as a catalysis substrate for fuel cells [45,58,59]. In these applications, using a small amount of metal does not significantly alter the electrical response of the underlying carbon nanofibers [18]. Thus this method could be used to fabricate metal-coated carbon nanofibers with varied amounts of metal, depending on the needs of the study and/or application.

In addition to the tunable metal coating, this approach is also flexible in terms of geometry and scale. While this approach was demonstrated here on vertically aligned carbon nanofibers grown on an electrode, free standing carbon nanofibers with high densities of edge plane carbon are commercially available. Given the availability of such materials, scaling up this approach and using varied geometries should be possible. There are several functionalization methods that can be used to add molecular monolayers to free standing carbon nanofibers [60], creating the anchoring sites for metal deposition. Coupling these methods with electroless deposition, as demonstrated here, will create a highly flexible materials platform useful in many varied applications.

Acknowledgments

This work was supported in part by the National Science Foundation Grant DMR-0210806.

References

[1] A.S. Arico, P. Bruce, B. Scrosati, J.M. Tarascon, W. Van Schalkwijk, Nat. Mater. 4 (2005) 366–377.
[2] R. Baughman, A. Zakhidov, W. de Heer, Science 297 (2002) 787–792.
[3] P.J.F. Harris, Int. Mater. Rev. 49 (2004) 31–43.
[4] P. Sharma, T.S. Bhatti, Energy Conver. Manage. 51 (2010) 2901–2912.
[5] E. Frackowiak, F. Beguin, Carbon 39 (2001) 937–950.
[6] J. Chen, F.Y. Cheng, Acc. Chem. Res. 42 (2009) 713–723.
[7] E.S. Steigerwalt, G.A. Deluga, C.M. Lukehart, J. Phys. Chem. B 106 (2002) 760–766.
[8] E.S. Steigerwalt, G.A. Deluga, D.E. Cliffel, C.M. Lukehart, J. Phys. Chem. B 105 (2001) 8097–8101.
[9] C. Kim, Y.J. Kim, Y.A. Kim, T. Yanagisawa, K.C. Park, M. Endo, M.S. Dresselhaus, J. Appl. Phys. 96 (2004) 5903–5905.
[10] M.D. Hughes, Y.J. Xu, P. Jenkins, P. McMorn, P. Landon, D.I. Enache, A.F. Carley, G.A. Attard, G.J. Hutchings, F. King, E.H. Stitt, P. Johnston, K. Griffin, C.J. Kiely, Nature 437 (2005) 1132–1135.
[11] M. Valden, X. Lai, D.W. Goodman, Science 281 (1998) 1647–1650.
[12] S. Arai, M. Endo, S. Hashizume, Y. Shimojima, Electrochem. Commun. 6 (2004) 1029–1031.
[13] Z.L. Liu, X.H. Lin, J.Y. Lee, W. Zhang, M. Han, L.M. Gan, Langmuir 18 (2002) 4054–4060.
[14] X.C. Ma, X. Li, N. Lun, S.L. Wen, Mater. Chem. Phys. 97 (2006) 351–356.
[15] Z.Q. Tian, S.P. Jiang, Y.M. Liang, P.K. Shen, J. Phys. Chem. B 110 (2006) 5343–5350.
[16] H. Vu, F. Goncalves, R. Philippe, E. Lamouroux, M. Corrias, Y. Kihn, D. Plee, P. Kalck, P. Serp, J. Catal. 240 (2006) 18–22.
[17] K.M. Metz, K.Y. Tse, S.E. Baker, E.C. Landis, R.J. Hamers, Chem. Mater. 18 (2006) 5398–5400.
[18] K.M. Metz, D. Goel, R.J. Hamers, J. Phys. Chem. C 111 (2007) 7260–7265.
[19] Y. Chen, Z.L. Wang, J.S. Yin, D.J. Johnson, R.H. Prince, Chem. Phys. Lett. 272 (1997) 178–182.
[20] A.V. Melechko, V.I. Merkulov, T.E. McKnight, M.A. Guillorn, K.L. Klein, D.H. Lowndes, M.L. Simpson, J. Appl. Phys. 97 (2005) 041301–041339.
[21] M. Meyyappan, L. Delzeit, A. Cassell, D. Hash, Plasma Sources Sci Technol. 12 (2003) 205–216.
[22] S.E. Baker, K.Y. Tse, E. Hindin, B.M. Nichols, T.L. Clare, R.J. Hamers, Chem. Mater. 17 (2005) 4971–4978.
[23] E.C. Landis, K.L. Klein, A. Liao, E. Pop, D.K. Hensley, A.V. Melechko, R.J. Hamers, Chem. Mater. 22 (2010) 2357–2366.
[24] S.E. Baker, P.E. Colavita, K.Y. Tse, R.J. Hamers, Chem. Mater. 18 (2006) 4415–4422.
[25] V.P. Menon, C.R. Martin, Anal. Chem. 67 (1995) 1920–1928.
[26] G. Socrats, Infrared and Raman Characteristic Group Frequencies: Tables and Charts, third ed., John Wiley & Sons, Ltd., New York, 2001.
[27] N.W. Alcock, V.M. Tracy, T.C. Waddington, J. Chem. Soc. Dalton Trans. (1976) 2243–2246.
[28] R.L. McCreery, in: A.J. Bard (Ed.), Electroanalytical Chemistry, Marcel Dekker, Inc., 1990, p. 221.
[29] R.J. Rice, R.L. McCreery, Anal. Chem. 61 (1989) 1637–1641.
[30] M.T. McDermott, C.A. McDermott, R.L. McCreery, Anal. Chem. 65 (1993) 937–944.
[31] Z. Kerner, T. Pajkossy, Electrochim. Acta 47 (2002) 2055–2063.
[32] B.D. Cahan, H.M. Villullas, E.B. Yeager, J. Electroanal. Chem. 306 (1991) 213–238.
[33] P.H. Chen, M.A. Fryling, R.L. McCreery, Anal. Chem. 67 (1995) 3115–3122.
[34] S.E. Baker, K.Y. Tse, C.S. Lee, R.J. Hamers, Diamond Relat. Mater. 15 (2006) 433–439.
[35] E.C. Landis, R.J. Hamers, J. Phys. Chem. C 112 (2008) 16910–16918.
[36] E.C. Landis, K.L. Klein, A. Liao, E. Pop, D.K. Hensley, A.V. Melechko, R.J. Hamers, Chem. Mater. 22 (2010) 2357–2366.
[37] G.O. Mallory, J.B. Hajdu, Electroless Plating: Fundamentals and Applications, American Electroplaters and Surface Finishers Society, Orlando, FL, 1990.
[38] C.J. Boxley, H.S. White, T.E. Lister, P.J. Pinhero, J. Phys. Chem. B 107 (2003) 451–458.
[39] H. Martin, P. Carro, A.H. Creus, S. Gonzalez, G. Andreasen, R.C. Salvarezza, A.J. Arvia, Langmuir 16 (2000) 2915–2923.
[40] H. Martin, P. Carro, A.H. Creus, S. Gonzalez, R.C. Salvarezza, A.J. Arvia, Langmuir 13 (1997) 100–110.
[41] S.S. Djokic, J. Electrochem. Soc. 144 (1997) 2358–2363.
[42] A. Kuhn, F. Argoul, J. Electroanaly. Chem. 397 (1995) 93–104.
[43] A. Kuhn, F. Argoul, J.F. Muzy, A. Arneodo, Phys. Rev. Lett. 73 (1994) 2998–3001.
[44] M. Nishizawa, V.P. Menon, C.R. Martin, Science 268 (1995) 700–702.
[45] M.A. Sanchez-Castillo, C. Couto, W.B. Kim, J.A. Dumesic, Angew. Chem. Int. 43 (2004) 1140–1142.
[46] Z.Z. Hou, N.L. Abbott, P. Stroeve, Langmuir 14 (1998) 3287–3297.
[47] T. Pajkossy, J. Electroanal. Chem. 364 (1994) 111–125.
[48] J. Bisquert, G. Garcia-Belmonte, F. Fabregat-Santiago, N.S. Ferriols, P. Bogdanoff, E.C. Pereira, J. Phys. Chem. B 104 (2000) 2287–2298.
[49] O.E. Barcia, E. D'Elia, I. Frateur, O.R. Mattos, N. Pebere, B. Tribollet, Electrochim. Acta 47 (2002) 2109–2116.
[50] R. de Levie, Electrochim. Acta 9 (1964) 1231–1245.
[51] G.J. Brug, A.L.G. Vandeneeden, M. Sluytersrehbach, J.H. Sluyters, J. Electroanal. Chem. 176 (1984) 275–295.
[52] S.R. Taylor, E. Gileadi, Corrosion 51 (1995) 664–671.
[53] K.Y. Tse, L.Z. Zhang, S.E. Baker, B.M. Nichols, R. West, R.J. Hamers, Chem. Mater. 19 (2007) 5734–5741.
[54] R. Jurczakowski, C. Hitz, A. Lasia, J. Electroanal. Chem. 572 (2004) 355–366.
[55] H. Shi, Electrochim. Acta 41 (1996) 1633–1639.
[56] G.J. Hutchings, M. Haruta, Appl. Catal. A 291 (2005) 2–5.
[57] M. Haruta, T. Kobayashi, H. Sano, N. Yamada, Chem. Lett. (1987) 405–408.
[58] A.C. Gluhoi, H.S. Vreeburg, J.W. Bakker, B.E. Nieuwenhuys, Appl. Catal. A 291 (2005) 145–150.
[59] W.B. Kim, T. Voitl, G.J. Rodriguez-Rivera, J.A. Dumesic, Science 305 (2004) 1280–1283.
[60] R.L. McCreery, Chem. Rev. 108 (2008) 2646–2687.